

## Scanning the Earth's Limb from a High-Altitude Balloon: The Development and Flight of a New Balloon-Based Pointing System

BRENDAN M. QUINE, KIMBERLY STRONG, ALDONA WIACEK, DEBRA WUNCH, JAMES A. ANSTEY, AND JAMES R. DRUMMOND

*Department of Physics, University of Toronto, Toronto, Ontario, Canada*

(Manuscript received 21 May 2001, in final form 4 October 2001)

### ABSTRACT

The development and first flight of a new balloon-borne pointing system is discussed. The system is capable of pointing a platform of optical instruments at an inertial target from a pendulating platform suspended below a high-altitude balloon. It operates in both a traditional occultation-scan mode, to observe solar absorption, and a limb-scan mode, to make measurements of Earth's limb. The system employs integrated sensors and high-level icon-based software (Labview). A microprocessor controller derives real-time estimates of gondola attitude, employing an extended Kalman filter to combine gyro, magnetometer, tilt-sensor, and shaft-encoder information. These estimates are used to develop control demands that point a platform of instruments in elevation and azimuth. The system's first flight was from Vanscoy, Saskatchewan, Canada, on 29 August 2000. Results of the system's performance during this mission are presented. In flight, the system demonstrated a pointing accuracy better than  $0.1^\circ$  ( $1\sigma$ ) in elevation and  $3^\circ$  ( $1\sigma$ ) in azimuth.

### 1. Introduction

Balloon-borne optical instruments have proved to be an important tool for probing the composition and state of the atmosphere. The primary advantage of making observations from a high-altitude platform is that instruments can be orientated to observe sections of a horizontally stratified atmosphere from near the ground to the observation altitude. Balloon missions provide a cost-effective means of making such observations in a timely manner.

In this paper we describe the development and first flight of a new balloon-borne pointing system, capable of pointing a suite of instruments with respect to an inertial reference frame from a pendulating platform. The system comprises a suite of sensors and actuators to provide two-axis attitude control, several instrument serial-communications channels for the command and control of instruments during flight, and a serial bidirectional ground communication interface providing telemetry transmission and a command capability. The complete system was developed in 14 months. This paper discusses the development of this pointing system and presents results from its first balloon flight.

### 2. Background

Most balloon pointing systems are developed to point a particular instrument. These systems may be categorized by the observational mode of the pointed instrument as either Sun-pointed or limb-pointed. Sun-pointed instruments operate in a solar occultation mode. During sunrise or sunset (when the Sun transits Earth's limb between the horizon and the platform's level plane), the pointing system tracks the Sun, enabling instruments to make measurements of solar absorption. The Sun provides a bright target reference, and these systems almost always use Sun-location sensors to provide direct measurements of pointing error for control. Typically, two approaches are adopted. Most commonly, a gondola system provides coarse azimuth control to orient the whole gondola to within a few degrees, and a mirror integrated with the instrument provides a two-axis (azimuth and elevation) fine control to track the Sun, with typical pointing accuracies quoted between  $\pm 0.017^\circ$  and  $\pm 0.3^\circ$ .

Zander et al. (1977), Farmer and Raper (1977), and Farmer et al. (1980) employed early systems of this type to point high-resolution spectrometers that measure atmospheric concentrations of hydrofluoric and hydrochloric acids and other constituents. Murcay (1984) and Murcay et al. (1983) developed a system with a sunseeker mounted above the gondola to give it an unobstructed view of the horizon and use it to point a Fourier transform spectrometer (FTS). Similar two-axis sun sensors were used to point a number of instruments during the Balloon Intercomparison Campaigns (BIC) of 1982

---

*Corresponding author address:* Dr. Brendan M. Quine, Department of Physics, University of Toronto, 60 St. George St., Toronto, ON M5S 1A7, Canada.  
E-mail: ben@atmosph.physics.utoronto.ca

and 1983 [see Watson et al. (1990) for a campaign overview and Carlotti et al. (1989), Farmer et al. (1990), Robbins et al. (1990), Roscoe et al. (1990), and Zander et al. (1990) for details regarding specific instruments]. The Geneva Observatory has developed a gondola with an azimuth-pointing specification of  $\pm 0.017^\circ$  (see Kopp and Huguenin 1995). It has been used to fly a number of limb-scanning instruments equipped with elevation-tracking mirrors, including the FTS occultation instrument LPMA (Limb Profile Monitor of the Atmosphere) and the stellar occultation instrument AMON (Absorption par Minoritaires Ozone et  $\text{NO}_x$ ) (see Hawat and Torguet 1996; Hawat et al. 1998; Payan et al. 1999).

The second approach is to rely on an accurate gondola-azimuth pointing and to employ only a single-axis elevation table or tracker. How (1980) describes an early gondola and table system with a pointing accuracy of  $\pm 0.05^\circ$  ( $3\sigma$ ).

Atmospheric spectra can also be recovered from infrared emission or ultraviolet scattered-sunlight measurements made during the day by scanning Earth's limb. Limb-scanning instruments can be employed to make continuous observations over a period of hours, producing measurement sets with a much higher temporal resolution than is possible with occultation-only instruments. The azimuth-pointing requirement for a limb-scanning instrument is less stringent than that for a sun-occultation instrument, as the limb has a large horizontal angular extent. Consequently, the pointing provided by the gondola is adequate for azimuth control, and instruments require only a single-axis tracking mirror to point at an elevation angle or tangent height corresponding to a particular atmospheric layer. The elevation-pointing requirement is similar, but control is more complicated, as there is no means to directly sense the observation target. Systems must therefore employ a variety of sensors to determine instrument attitude and rely on careful calibration to relate this to the instrument-pointing direction. One approach is to neglect the effect of gondola pendulation over the duration of each scan sequence and then to recover an estimate of the horizon location in postprocessing.

Waters et al. (1981, 1984) have developed a balloon-borne microwave limb sounder (BMLS) with an elevation mirror that is stepped in  $0.2^\circ$  increments. Scan angles are referenced to tangent height by observing the increase in  $\text{H}_2\text{O}$  emission at the tropopause. Abbas et al. (1987) and Brasunas et al. (1988) describe SIRIS, an FTS instrument with a single-axis scan mirror. Elevation offset is measured using an inclinometer and verified by a postflight analysis of measured  $\text{CO}_2$  lines. Drummond et al. (1986) describe a limb-scanning instrument flown in 1983 on an uncontrolled gondola that simultaneously scanned opposing sides of Earth's limb. In the absence of severe pendulation, an elevation reference is derived by comparing opposing limb measurements under an assumption that the atmosphere is horizontally homogeneous.

Another approach is to employ an elevation controller with a gyro sensor and stabilize elevation pointing. The Smithsonian Astrophysical Observatory developed an instrument with a pointing accuracy of  $\pm 3^\circ$  in azimuth and  $\pm 0.02^\circ$  in elevation (see Johnson et al. 1995; Chance et al. 1996), and the Institut für Meteorologie und Klimaforschung developed a star-referenced pointing system for an instrument called the Michelson Interferometer for Passive Atmospheric Sounding (MIPAS-B) with a pointing accuracy of  $\pm 0.08^\circ$  ( $3\sigma$ ) and a postprocessed pointing knowledge of  $\pm 0.016^\circ$  ( $3\sigma$ ) (see Oelhaf et al. 1991; Seefeldner and Keim 1995; Maucher 1995).

In this work, we describe the development of a complete two-axis gondola pointing system capable of pointing a platform of instruments along a common line of sight. The system includes both a sun-occultation mode and a limb-scanning mode. The ability to coalign a number of instruments along a common atmospheric path has several advantages. First, a range of different instruments and techniques may be employed during the same mission, and a larger number of atmospheric constituents may be recovered simultaneously along the same optical path, producing a more complete picture of atmospheric state and chemistry. Second, similar instruments, or instruments making similar measurements, may be coaligned to allow for a direct comparison of results: newly developed instruments may be compared with existing standard techniques, and identical instruments may be compared to gain an understanding of instrument variability and retrieval accuracy. Third, a range of optical measurement techniques may be directly compared in order to resolve some of the large profile discrepancies routinely reported by instruments observing important species such as ozone. Last, a pointing-mirror control system is not required on an instrument-by-instrument basis, simplifying the development of balloon-borne instrumentation.

### 3. High-altitude ballooning

High-altitude balloons reach a typical altitude of 25–45 km, depending on payload mass, balloon size, and gas volume. For all but the smallest payloads, launch and flight operations are provided by a launch contractor, who typically provides launch facilities, ground-to-balloon communications, gondola power, and flight services, including termination and recovery.

Figure 1 shows a typical flight configuration. A box-section gondola containing instruments, batteries, and electronics subsystems is suspended on a long flight train below the balloon. Working from the base upward, the flight train consists of the following elements.

- A gondola rotational mount, attached to the gondola corners by suspension cables, and incorporating drive motors, provides azimuth gondola control.
- A mass boom provides some additional inertia to stiff-

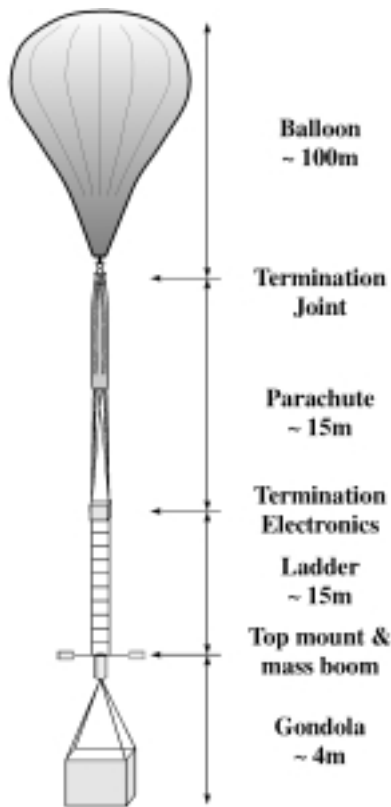


FIG. 1. Typical flight train.

en the flight train and provide resistance to azimuth torque.

- A steel-cable ladder of length approximately 15 m, with rungs spaced 1 m apart and of width 0.3 m, extends the distance between balloon and payload to prevent the balloon from shadowing instruments or substantially distorting the airflow around the gondola (which might affect in situ sampling instruments).
- A termination electronics box provides independent telemetry and drivers for the pyrotechnic termination device.
- A parachute of approximately 15 m is rigged to deploy when the payload is separated from the balloon.
- A termination joint consisting of a yoke and mandrel held together with a steel-cable binding is equipped with pyrotechnic cable cutters to release the binding on ground command.
- A mount interfaces the balloon and the termination joint.

The gondola dynamics are dominated by a complex pendulum motion of the flight train about pivot points at the base of the balloon and at the top mount. This effect is particularly evident at launch, when the release of the gondola and balloon acts to drive this motion. As there is little damping in the flight train, pendulation induced by launch can take several hours to subside but has usually disappeared by the time the balloon reaches float

altitude. At float altitude, wind-shear forces acting on the balloon also drive this type of motion, inducing oscillations that can be as large as  $1^\circ$  in both azimuth and elevation (Hawat and Torguet 1996).

Torques generated by control actions also act to excite the payload dynamics. While the suspension system is relatively insensitive to control torques driving an elevation stage within the gondola, the cable ladder in the lower flight train provides relatively little instantaneous resistance to azimuth control torques. A control torque applied to the azimuth mount acts to “wind up” the flight train, shortening its length and raising the payload. In the absence of any mechanical damping, the energy associated with a control maneuver is stored as rotational potential energy. This effect induces an oscillatory motion at a period associated with the rotational spring constant of the cable ladder and acts to complicate azimuth control considerably. Free-play in the interconnections of the flight train (particularly the balloon connection) and stiction in the top-mount bearing exacerbate this effect. The addition of the mass boom at the base of the flight train increases the period of the motion but does not remove the effect. Some systems, such as the Geneva Observatory gondola, opt to avoid this control problem entirely by including an additional rotational pivot above the mass boom to decouple the ladder dynamics. In this configuration, the boom behaves like a momentum wheel, opposing control torques by storing angular momentum as boom rotational motion.

Balloon systems must operate under a range of harsh environments. During ascent, systems cool rapidly as they pass through the tropopause and, if unprotected, may cool to as low as  $-40^\circ\text{C}$ . At float altitude during the day the Sun provides a large heat input, and systems can reach  $55^\circ\text{C}$ . At night, systems cool again as they radiate energy to space. Since at float altitude the ambient pressure is less than 1000 Pa, there is little convective cooling, and thermal designs must use conductive or radiative solutions.

Balloon systems usually have conservative mass and power requirements. Systems with large power requirements incur a mass penalty in additional battery packs and also increase thermal design problems. Heavier payloads may also require a larger balloon, more lift-gas, and heavier flight-train fittings.

The vibration environment of a balloon system is benign, but systems must still survive motion during launch as the truck maneuvers to release the payload directly under the balloon. The descent at the end of the mission can apply large shocks to balloon systems—the payload may free-fall for some time before the air pressure increases enough to open the parachute. The U.S. National Scientific Balloon Facility (NSBF) requires flight-train fittings to be rated for a worst-case 10-g shock, but this requirement is rarely applied to other balloon systems. Landing may also induce a considerable shock. Due to the unpredictability of the land-

TABLE 1. Pointing requirements.

| Mode          | Axis      | Pointing requirement<br>( $1\sigma$ accuracy; $1\sigma$ knowledge) |
|---------------|-----------|--|
| Sun pointing  | Elevation | $\pm 0.1^\circ$  |
|               | Azimuth   | $\pm 0.1^\circ$  |
| Limb pointing | Elevation | $\pm 0.1^\circ$  |
|               | Azimuth   | $\pm 1.0^\circ$  |

ing site and shocks involved, balloon systems are rarely designed with an explicit requirement to survive the descent, although most systems are designed to be reusable.

#### 4. Pointing system requirements

The pointing system would be required to point a suite of instruments with a combined mass of up to 75 kg (with a moment of inertia not exceeding  $15 \text{ kg m}^2$ ) in two axes—azimuth and elevation. Heavier instruments could also be coaligned by the use of mirrors mounted so as to direct radiation along the pointing system elevation axis. The system would be able to point  $0^\circ$  to  $360^\circ$  in azimuth and at least  $-10^\circ$  to  $+50^\circ$  in elevation (referenced from the level-pointing plane). The system would be capable of maintaining tracking at a maximum gondola rotation rate of  $2^\circ \text{ s}^{-1}$ . The system would operate in an ambient environment ranging between  $-70^\circ$  and  $+55^\circ\text{C}$  and under a pressure range from one atmosphere ( $\sim 10^5 \text{ Pa}$ ) to 100 Pa. It would draw power from an unregulated single voltage  $+28 \text{ V}$  supply, consuming less than 200 W (including drive motors) and with a peak current of less than 10 A. It would weigh less than 50 kg (excluding the top mount).

The system would include two principal operational modes: a Sun-pointing mode and a limb-scanning mode. Table 1 lists the pointing requirements identified for each mode. While in Sun-pointing configuration, the pointing requirement is driven by the need to keep the field of view of each pointed instrument fully illuminated. Given that the angular diameter of the Sun is  $0.5^\circ$ , an instrumental angular field of view of  $0.1^\circ$  may be confined to the solar disk within acceptable confidence bounds, if the pointing accuracy exceeds  $\pm 0.1^\circ$  ( $1\sigma$ ). This pointing requirement is therefore adopted for this development. A more stringent requirement might well improve instrument results by further confining the field of view to a subsection of the solar disk, but this is not a core requirement. For some instruments these requirements could be considerably relaxed (instruments employing front-end diffusers typically require a pointing accuracy of only a few degrees).

While in limb-pointing configuration, the elevation requirement of  $\pm 0.1^\circ$  is driven by a requirement for a 2-km vertical resolution in recovered spectra. Since the limb is relatively featureless in the horizontal, the azimuth requirement can be relaxed and a pointing requirement an order of magnitude less than the elevation

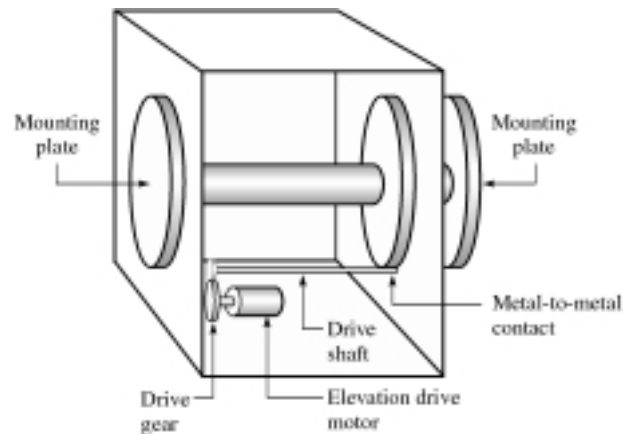


FIG. 2. Schematic of pointing system elevation components.

requirement is adopted. This mode would also need to include an automated scan configuration that would perform a sequence of scans at different elevation angles or tangent heights without continuous ground intervention. Additional control modes to point at a particular orientation and to exercise the system are required for system diagnosis and testing.

Pointing system communication and control would be via a bidirectional RS-232 serial link connected to the ground via a multiplexor and using S-band transmission equipment provided by the flight contractor. Transmitter limitations require that the downlink data rate would be limited to 9600 baud and that the uplink data rate would be less than 30% of a 300-baud link. All critical data would be sent to the ground in real time in data packets with checksums. Command and control of the system would be via occasional command transmitted in small data packets, also with checksum verification. The pointing system would also include additional RS-232 ports for instrument communication to initiate instrument scans and to change instrument modes.

#### 5. Hardware development

The pointing system makes as much use of existing hardware as possible. A previous pointing system with a single Sun-occultation mode had been developed in the late 1970s by the launch contractor. The control electronics from this system could not be adapted to include a limb-scanning mode, but the gondola structure and the azimuth top mount (including redundant analog drive motors) are used since both have a considerable flight heritage.

For the elevation drive, a mechanical unit developed by the Meteorological Service of Canada (MSC) to point ground-based instruments proved adaptable. Its key advantage is a final drive gear with a direct metal-to-metal contact that eliminates backlash.

Incorporating these original components, the new sys-

tem's mechanical hardware consists of an aluminum housing containing a central 150-mm-diameter tube and bearings for rotation in elevation. Instrument-mounting faces are bolted externally to the tube ends, and a metal drive disk is mounted internally. This disk is driven by a stepper motor (Slo-Syn MO63-FC06) through a flex-coupling and a 100:1 gear with a 20-mm drive rod held in metal-metal contact with the disk by a spring mechanism. A schematic of these elevation drive components is shown in Fig. 2. A shaft encoder (Gurley), measuring absolute angular position with 16-bit resolution, is mounted inside the tube via a flex-couple to give the angle of the elevation stage with respect to the pointing system case. Optical limit switches connected to the stepper drive unit prevent tube rotation beyond  $-25^\circ$  and  $+65^\circ$  in elevation. Elevation action is produced by serial command to a programmable stepper motor controller (Applied Motion 3540i). The controller includes microstepping, current-limiting, and limit-switch activation via software command. Figure 3 shows the pointing system housing with an inspection cover removed to reveal the elevation drive mechanism. The gondola is controlled in azimuth using two motor-drive amplifiers (Inland EM-1803) bolted inside the pointing system housing that develop a torque proportional to an analog signal voltage applied. Two circuits are included for redundancy.

The pointing system includes a set of sensors to measure the attitude of the gondola. A three-axis magnetometer (Crossbow 539), mounted on a 1-m aluminum boom away from the stainless steel suspension cables, senses Earth's magnetic field. A tilt sensor (Crossbow CXTILT02E) is also included and measures the gondola's tilt in two axes. This sensor is included to provide a vertical reference but cannot be used directly for gondola control since gravity-referenced sensors are insensitive to pendulum motion. Both sensors include temperature compensation circuitry and receive commands via serial lines.

The most critical gondola attitude sensor is a two-axis gyro (Litton G2000). The gyro develops a voltage signal proportional to the rotation rate in the azimuth and elevation axes but, in common with other high-accuracy gyros, also has a zero offset that is highly temperature dependent. Since the output of this gyro must be effectively integrated to measure angle, this offset must either be characterized or be carefully controlled to limit short-term variations. Laboratory thermal tests with the gyro determined that this offset was not entirely repeatable from test to test; it was therefore decided to control the gyro temperature carefully rather than attempt to characterize the drift as a function of temperature. The gyro is mounted on an aluminum block in a thermal enclosure with a temperature sensor and a Kapton heater. A control loop with a programmable set temperature provides thermal control, but, as will be discussed later, the thermal design renders strict temperature control unnecessary, because the gyro temper-

ature drift is slow enough during flight to allow the characterization of gyro offset using other sensors.

The gyro outputs are amplified to increase rate resolution and are then filtered through a second-order analog Bessel filter, tuned at 100 Hz, before they are sampled using a 16-bit data-acquisition (DAQ) channel. This conditioning limits the maximum sensed rate to  $\pm 10^\circ \text{ s}^{-1}$  and gives a resolution of  $3 \times 10^{-4} \text{ s}^{-1}$ .

In order to accommodate a Sun-pointing occultation mode, the elevation platform is instrumented with two one-axis Sun sensors from the previous pointing system. They consist of an input slit with an optical filter to reduce the Sun's power and two sets of opposed solar cells wired in opposition. One set, mounted near the slit, is used for coarse sun location over a  $\pm 50^\circ$  range, and one set is mounted farther away from the slit and provides fine Sun location within a  $\pm 5^\circ$  range. Both ranges produce an output voltage of up to  $\pm 5 \text{ V}$ , roughly proportional to the sun offset, although both ranges are highly nonlinear when the Sun is off-axis (where the gain can change by as much as a factor of 3). The two sensors are mounted so as to provide sun-offset location in elevation and azimuth with respect to the pointing platform.

The system also includes sensors for measuring temperature, pressure, and location. Two pressure sensors (Honeywell 142PC15A), mounted internally and externally, make crude measurements of air pressure to within a few hundred pascals and are directly sampled. An additional temperature sensor makes a crude measurement of air temperature. The system also includes a global positioning system (GPS) receiver (Garmin GP-35) to provide location and altitude data. This unit is interfaced to the pointing system using a serial channel but was not used during the first flight.<sup>1</sup>

The pointing system is controlled by a single-board microprocessor mounted inside the pointing system housing (a Pentium III 500EB 12-W processor mounted on a motherboard card with 128 MB of RAM). The microprocessor system includes keyboard, video, and Ethernet interfaces for ground test. The system interfaces with pointing-system sensors and other hardware using 12- and 16-bit DAQ channels and a total of 10 RS-232 ports. The system requires +5 V (main system power) and  $\pm 12 \text{ V}$  rails (required for RS-232 communications). A schematic of the hardware configuration is shown in Fig. 4. The operating system and flight code are stored on a 2.5-in. hard drive mounted in a pressure housing. A single custom-fabricated electronics interface board, mounted in the computer, contains all the required interface circuitry within the pointing system. This card includes the gyro-conditioning electronics, a programmable logic device (PLD) to handle sam-

<sup>1</sup> A GPS antenna of this type was flown during the flight but was interfaced with another system. The antenna functioned nominally during the flight, apart from a brief loss of track during the ascent caused by excessive thermal cooling due to a lack of insulation.

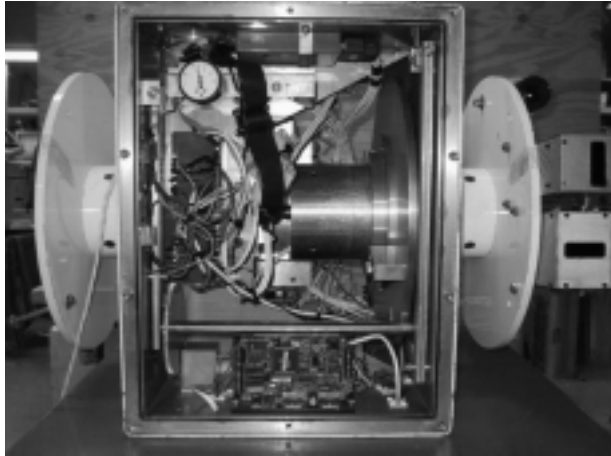


FIG. 3. Pointing system with front cover removed showing Sun sensors (far right), instrument mount disks (left and right), central shaft assembly, metal-metal drive (bottom right), stepper motor driver (bottom), azimuth drive amplifiers (center left), and pressurized hard drive casing (top left).

Since the pointing-system housing is unpressurized, special consideration is given to the system's thermal design. Traditional computer convective-cooling solutions cannot be employed in near-vacuum operations, in which only conductive and radiative schemes are effective. The majority of the power dissipation occurs within the processor itself. A 25 mm<sup>2</sup> aluminum block is bonded directly to the processor integrated circuit (IC). The block is then interfaced to the base of the pointing system housing, providing a substantial thermal path for heat dissipation. Heat dissipation by other components is substantially less, although in initial tests some ICs exceeded 80°C under vacuum conditions. These ICs are therefore cooled using a flexible thermal epoxy (TRA-CON BA-813J01) spread over the component surfaces of the boards to increase the heat dissipation surface. This epoxy is sufficiently thermally conductive to spread the thermal load but flexible enough to be removed if needed. Under vacuum testing, it cooled hotter components by more than 20°C.

ple timing for the shaft encoder, a four-channel programmable heater driver, buffered digital input and output lines, and interface wiring for all serial connections and sensors. The cards are mounted within a cage to secure them during launch.

The main pointing system power is supplied from a dc/dc switcher (VICOR) rated from -25°C to +85°C and developing two 50-W channels, +5 V and +28 V, from an 18- to 36-V input. The power supply includes thermal and voltage overload protection and also isolates the system from voltage variations caused by other

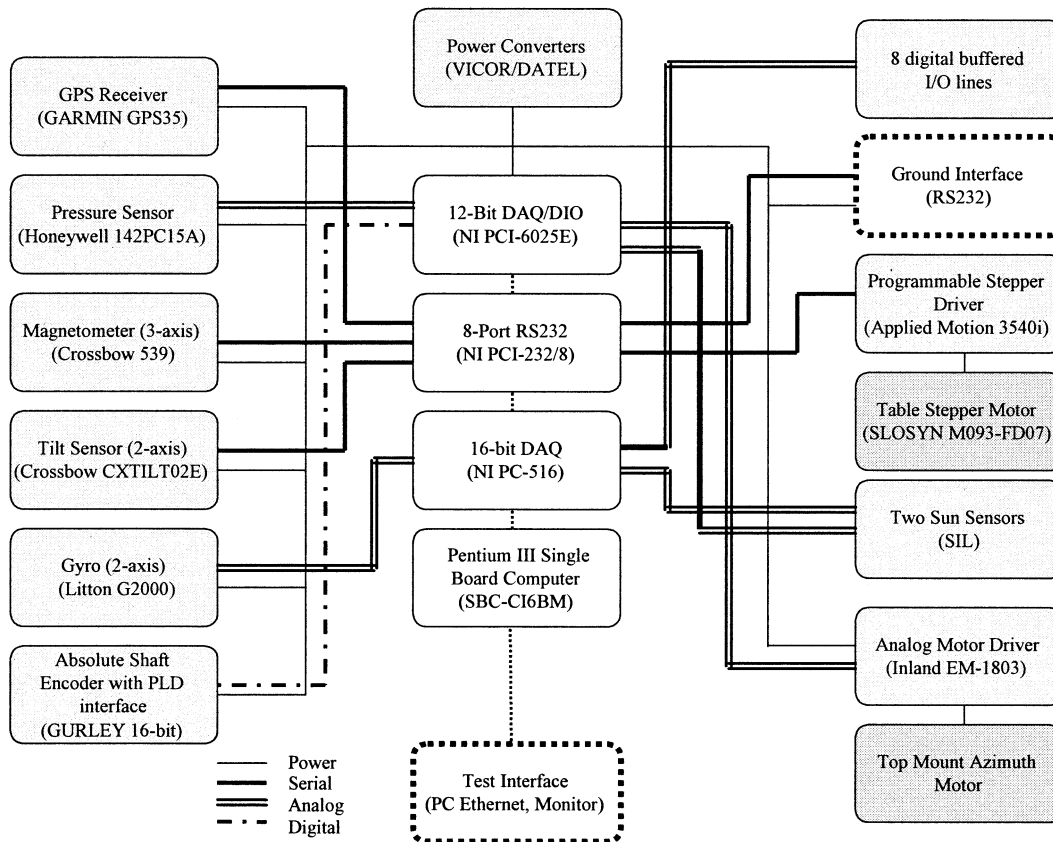


FIG. 4. Pointing system hardware configuration.

balloon systems and battery discharge. Additional low-power  $\pm 12$  V power rails are developed by a smaller dc/dc converter (DATEL BWR-12/625-D5A) from the +5 V rail for the RS-232 ports.

## 6. Software development

The pointing system requires a real-time flight code to sample sensors, develop control demands, and communicate with the ground and other instruments. Traditionally, this code would be developed in a low-level language such as C or Ada in an emulation environment, on another platform, which would provide a user interface and a range of development tools, such as debuggers, and only ported to the flight hardware for testing. Given the short timeline of the pointing system project, we opt to develop the software entirely on the flight hardware and utilize the microprocessor's high capacity to run a conventional Windows-based operating system (Microsoft Windows 98) and take advantage of high-level software development tools (National Instruments' Labview).

Labview is an icon-based graphical development language, especially designed for hardware interface tasks. In contrast with a traditional script-based language, modules are developed in two panels: one containing icons representing inputs, outputs, and controls of the module and one containing subfunctions, data operations, sequencing, and wiring to represent the flow of data. Labview executes modules hierarchically in pseudoparallel, and, consequently, any ordering or sequencing must be explicitly defined. Labview includes an extensive library of functions and interface drivers for a wide range of DAQ and communication hardware.

The pointing system flight code is developed in several stages. First, a set of three modules is developed to initialize, read, and convert data for each sensor. A Boolean flag is included to indicate if the sensor fails to initialize. This flag is used to prevent delays in sequenced operations caused by a faulty sensor. Another Boolean flag indicates whether data is valid, applying checksum and range checks to prevent faulty data from further processing, which might corrupt the pointing system's attitude estimate. Equivalent modules are also developed to initialize and to command the elevation and azimuth motors.

Second, a test module is developed that includes all of the sensor and actuator interfaces. This module samples the sensors and generates actuator demands in closed loop, using a very simple single-sensor control approach in order to verify that the sensors and actuators may all be controlled in tandem.

Third, an estimator module is developed, based on the Kalman stochastic estimation. This module includes all the subfunctions required to process the gyro, tilt, and magnetometer sensor data into a single estimate of gondola attitude and is discussed further in the next section.

TABLE 2. Pointing system commands.

| Command | Description                               | Data format   |
|---------|---|---|
| MP      | Modify a pointing system parameter        | 1-byte integer parameter number<br>4-byte single precision real |
| MB      | Modify a Boolean state                    | 2-byte word containing all Boolean states                       |
| SP      | Send a raw data-string to instrument port | 5-byte string of data to be written                             |
| IS      | Initiate a sensor or scan                 | 1-byte integer to indicate which sensor or scan table type      |
| SH      | Initiate pointing system shutdown         | None  |

Fourth, downlink and uplink transmit and receive modules are developed. In order to ensure that data can be analyzed after flight, both raw sensor data and pointing system operational data are transmitted to the ground during every cycle of the pointing system's control loop. The data are transmitted in fixed length packets of 8-bit bytes, each packet starting with two synchronization bytes (ASCII characters 205 and 170) and ending with a checksum byte consisting of the byte of sum of all the bytes in the packet. Two other datasets—noncritical sensor data and pointing system configuration data—are downlinked serially, one element per cycle, in order to conserve downlink bandwidth.

Labview is also employed in the ground-station software, and this code shares common modules with the flight software. The command uplink code works in a similar fashion with commands packed into 10-byte strings, including synchronization and checksum. Commands must pass the checksum before they are executed and are returned to the ground as verification. Table 2 describes the commands that are implemented.

Finally, the main flight code is developed, incorporating the modules into a single program. The main control loop runs at 7 Hz, timed from the gyro DAQ. The gyro is sampled twice per loop cycle to ensure that gyro rates have an adequate temporal resolution to capture dynamic motion. The loop includes an automated event-handler mode. A table of events may be loaded into the event handler, by ground command, which then executes them sequentially. Several event types can be automated, including commands to point at a particular target orientation, to initiate an instrument scan and to change the pointing mode. Execution conditions and a postexecution delay may be set for each event. A flag may also be set to require that the pointing platform be on target before the next event can be executed. The on-target criterion is based on a fading memory average of the pointing error, computed at each filter cycle, with time-constant and pointing-accuracy parameters that are programmable from the ground.

An asynchronous loop executes at a 2-s cycle and sequences through three non-time-critical tasks: a gyro thermal-control module computes heater demands to

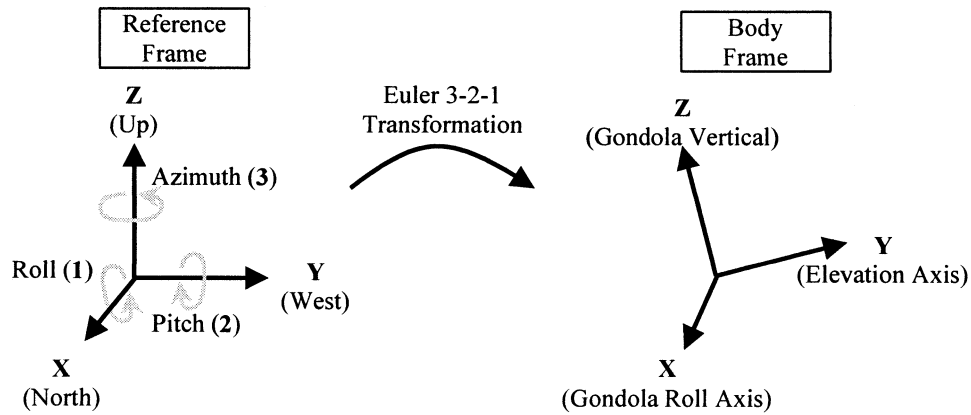


FIG. 5. A diagram to illustrate axis frame conventions and Euler 3–2–1 transformation.

stabilize gyro temperature, a command execution module receives and executes ground commands, and an instrument communication module generates the command-timing sequences to initiate an instrument mode or scan.

The flight code is configured to start automatically at power up as part of the operating-system boot sequence. The computer basic input–output system (BIOS) is configured to power down the hard disk 5 min after boot to conserve power and to prevent hard disk damage during launch. The flight code also includes a ground command to initiate a controlled system shutdown after a 10-s delay.

## 7. Attitude estimation and control

The pointing system employs a stochastic Kalman filter–type estimator to calculate a real-time estimate of the gondola attitude for use in limb scanning. Kalman filter estimators are widely employed to make real-time estimates of location or attitude for a large variety of autonomous vehicles (see Jazwinski 1970; Wertz 1978; Maybeck 1979; Cambell 1983; Chui and Chen 1987; Durrant-Whyte 1988). They propagate a time-evolving vector of parameters describing the expected state of the system, incorporating new observation data at each update cycle. They require a state evolution model that predicts how the state estimate evolves in time and a sensor or observation model that predicts an expected vector of observations given a particular state vector. The estimator uses these models to propagate a probabilistic representation of the expected true state, based on mean and covariance statistics. At each cycle, the estimator projects the current state estimate forward in time and generates an observation residual from the difference between measured sensor observations and estimate-based observation predictions. This residual is used to correct the state estimate, weighting the new sensor information into the current estimate and minimizing the mean-squared error according to covariance

models of the expected observation noise, the estimated state noise, and the expected state prediction noise.

Kalman filter estimators divide into two classes. Linear Kalman filters can be used in problems in which all models are linear and can be reduced to a simple matrix form (Kalman 1960). Extended Kalman filters are adaptable to problems where one or more system model is nonlinear. These filters operate by locally linearizing models about the state prediction at every filter cycle. As we shall discuss, the observation models needed to estimate the gondola attitude are nonlinear, and a filter of this latter type is therefore required.

In this work, we employ a variant of the traditional nonlinear algorithm (see Quine 1997; Quine 1999, manuscript submitted to *Automatica*; Quine et al. 1995). This filter variant can be configured to produce results identical to the more traditional algorithm but has a significant implementation benefit: it does not require the analytical computation of model partial derivative (or Jacobian) matrices.

Gondola attitude must be computed with respect to an inertial reference frame. In this work, we adopt an Euler 3–2–1 description of attitude with respect to a Cartesian reference frame. Figure 5 illustrates the three-axes definitions for both the reference and body frames. An Euler 3–2–1 attitude description maps the reference frame to the gondola body frame using three successive rotations about the third, second, and first axes (or  $z$ ,  $y$ , and  $x$  axes). We further reduce this attitude description to two dimensions by ignoring rotations about the  $x$  or gondola roll axis and by defining a rotation about the  $z$  axis as an azimuth rotation and a rotation about the  $y$  axis as an elevation rotation. This reduction is legitimate since, rather than estimating gondola attitude, we seek to point a platform of instruments at a largely horizontally stratified target. We can reasonably expect a suspended gondola to have an attitude confined within  $\pm 1^\circ$  in the elevation and roll axes. Small rotations about the gondola roll axis will induce only very small errors in

apparent elevation, which will not significantly affect pointing performance.

The Kalman filter estimates a six-element state vector consisting of angle, angular rate, and gyro drift for the elevation and azimuth axes:

$$\hat{\mathbf{x}}(k) = \begin{bmatrix} \phi \\ \dot{\phi} \\ \delta_\phi \\ \theta \\ \dot{\theta} \\ \delta_\theta \end{bmatrix}, \quad (1)$$

where  $\hat{\mathbf{x}}(k)$  is the state estimate at time step  $k$ ;  $\phi$ ,  $\dot{\phi}$ , and  $\delta_\phi$  are the azimuth angle (rad), angular rate (rad s<sup>-1</sup>), and azimuth gyro drift (rad s<sup>-1</sup>), respectively; and  $\theta$ ,  $\dot{\theta}$ , and  $\delta_\theta$  are the elevation angle, angular rate, and elevation gyro drift in corresponding units. Each axis is assumed to be uncoupled, and the state-evolution models are assumed to be linear. The model can therefore be expressed as a matrix  $\mathbf{F}$ :

$$\mathbf{F} = \begin{bmatrix} 1 & \Delta t & 0 & 0 & 0 & 0 \\ 0 & 1 & 0 & 0 & 0 & 0 \\ 0 & 0 & 1 & 0 & 0 & 0 \\ 0 & 0 & 0 & 1 & \Delta t & 0 \\ 0 & 0 & 0 & 0 & 1 & 0 \\ 0 & 0 & 0 & 0 & 0 & 1 \end{bmatrix}, \quad (2)$$

where  $\Delta t$  is the time between filter cycles (s). The state prediction is therefore expressed as  $\mathbf{F}\hat{\mathbf{x}}(k)$ . The Kalman filter incorporates magnetometer, gyro, and tilt-sensor data. The tilt-sensor data is used only in elevation and has a lower weighted significance since the sensor cannot sense any dynamic pendulum motion and only serves to derive a static elevation offset. The filter also includes an observation of a fading-memory average of the azimuth gyro rate to help derive an azimuth gyro drift (measured only during periods of low-rate static pointing). These latter two observations are required to aid the determination of gyro drifts at particular attitudes. When Earth's magnetic-field axis is normal to the roll axis (when the gondola points roughly east or west), then rotations in azimuth and elevation cannot be easily distinguished using magnetometer data alone, and, consequently, the filter is unable to distinguish between changes in gyro drift and gondola motion. In this configuration, the filter is unstable and strongly divergent without additional data, and the attitude-state vector is unobservable. The addition of the tilt-sensor elevation observation and the observation of the fading averaged azimuth rate provides enough information to prevent this instability and allows the filter to estimate through these regions. The Sun sensors are not used for limb control because they are highly nonlinear when the Sun is not boresighted. Stacking the observations into a single vector  $\mathbf{z}(k)$ , the observation vector can be expressed as

$$\mathbf{z}(k) = \begin{bmatrix} m_x \\ m_y \\ m_z \\ g_\phi \\ g_\theta \\ t_\theta \\ \bar{r}_\phi \end{bmatrix}, \quad (3)$$

where  $(m_x, m_y, m_z)$  is the direction of the magnetic-field vector in the body frame,  $g_\theta$  and  $g_\phi$  are the gyro-rate observations,  $t_\theta$  is the tilt-sensor observation, and  $\bar{r}_\phi$  is the fading-memory average of the azimuth-rate observation. The expected observation  $\hat{\mathbf{z}}(k)$  can be expressed in terms of an observation model  $\mathbf{H}$  as

$$\hat{\mathbf{z}}(k) = \mathbf{H}[\hat{\mathbf{x}}(k), m^0] = \begin{bmatrix} \cos(\phi)m_x^0 + \sin(\phi)m_y^0 \\ -\sin(\phi)m_x^0 + \cos(\phi)m_y^0 \\ m_z^0 \\ \dot{\phi} + \delta_\phi \\ \dot{\theta} + \delta_\theta \\ \theta \\ \delta_\phi \end{bmatrix}, \quad (4)$$

where  $m^0 = (m_x^0, m_y^0, m_z^0)$  is the direction of the magnetic-field vector in the reference frame and is derived experimentally in preflight suspension tests. The original intention was to use elevation estimates in the magnetometer model, but this complexity is omitted because magnetic field measurements are found to deviate significantly from a simple single-field model and tend to corrupt the elevation estimate. This deviation is likely attributed to an unmodeled magnetic-field component associated with magnetic equipment on the gondola (the process used in the manufacture of high-strength, stainless steel suspension wires is known to magnetize them). As a consequence, the  $z$ -axis magnetometer measurement has very little informational value and could be omitted from the observation vector.

The observation noises are directly computed from sensor data recorded during a static-pointing test. Each measurement is assumed to be uncorrelated with any other except for the three magnetometer axes, which are assumed to be coupled due to normalization of the magnetic vector. The gyro noise is set to 10<sup>-4</sup> rad s<sup>-1</sup>, the gyro drift noise to 10<sup>-6</sup> rad s<sup>-1</sup>, and the fading average azimuth-rate observation noise to 10<sup>-6</sup> rad s<sup>-1</sup>. The tilt-sensor noise term is set to 10<sup>-2</sup> rad, an order of magnitude higher than the actual sensor noise to reduce its significance in the estimate. The magnetometer noise term was also increased from its measured value of 4 × 10<sup>-4</sup> to 2 × 10<sup>-2</sup> rad to compensate for uncertainties in the simple magnetic-field model. The evolution-model noise term is harder to compute, and instead this term is tuned in performance testing of the complete system (a value of 10<sup>-6</sup> rad s<sup>-1</sup> was used in post-data processing).



FIG. 6. Pointing system mounted in gondola frame in the flight configuration with the SPS instrument (left), pointing system housing (center), and sun sensors (right).

Two independent axis-control laws compute the required control action from the pointing error. In limb mode, this error signal is computed as the difference between the required gondola attitude and the estimated attitude. In Sun mode, the system uses only Sun sensors for control, and the error signal is simply the Sun offset measured by the Sun sensors and converted into degrees. The pointing system uses simple bounded proportional, integral, differential (PID) controllers to generate actuator demands to control the gondola. The PID algorithms are conventional, except that the size of the integral term is bounded to prevent it from diverging during dynamic motion. The PID controller weights are also tuned during performance testing. All Kalman filter and controller parameters may be adjusted during flight.

## 8. Thermal and performance testing

All flight systems were vacuum tested prior to flight to ascertain their performance under conditions similar to their operational environment. The performance of each sensor was evaluated in a static test to determine sensor-noise characteristics and in a dynamic test to set sensor gain characteristics. After the pointing system hardware was completed and integrated with the gondola, extensive dynamic performance tests are performed in the laboratory using an alignment laser to verify pointing performance in elevation. The complete system was also tested in the field, suspended from a 30-m crane, in order to simulate a realistic pendulum length and typical dynamical motion at float altitude. Before flight, the pointing system was aligned with other instruments using the Sun as a reference and calibrating the magnetometer using a Sun-location algorithm developed by Walraven (1978) and a time calculation given by Michalsky (1988).

TABLE 3. A log of flight events during the MANTRA 2000 mission.

| Time (UTC) | Log entry   |
|------------|---|
| 0832       | Switch on pointing system (first data 894 s before launch).                                       |
| 0845:20    | Launch.   |
| 0907       | Reinitialized the Kalman filter—OK now.   |
| 0909       | Switched on gyro heater and set temperature to 30°C.  |
| 0921       | Switched on azimuth control mode 4.   |
| 0922       | Solar pointing engaged ready for sunrise.   |
| 1134:00    | Sun pointing acquisition (on sun acquisition: elevation better than 0.1, azimuth $\pm 6^\circ$ ). |
| 1256       | Switched azimuth motors off.  |
| 1310       | Stopped data collection.  |
| 1311       | Restarted data collection.  |
| 1353:40    | Started autonomous limb scan (Table 4, SPS mode 2)—killed by relay switch.                        |
| 1422:00    | Started autonomous limb scan (Table 4, SPS, mode 2).  |
| 1530       | Commands down (no command capability for rest of mission).  |
| 2229       | Last pointing system data received.   |

## 9. First flight

The pointing system was flight tested during the Middle Atmospheric Nitrogen Trends Assessment (MANTRA) 2000 balloon flight. The balloon was launched in the early morning from Vanscoy, Saskatchewan, Canada, at 0845:20 UTC 29 August 2000. Figure 6 shows the pointing system just prior to the flight, fully integrated with the gondola. A sun photospectrometer (SPS) instrument, developed by McElroy (1995) and the MSC, was mounted on the pointing platform. This instrument was used to evaluate pointing system performance and collect spectral data in two ranges, from 280 to 385 and 385 to 780 nm, in order to measure ozone, NO<sub>2</sub>, O<sub>2</sub>, and aerosols. The SPS has a sufficient dynamic range to be used in both occultation and limb-pointing modes. During limb scanning, this instrument operated under direct command from the pointing system in order to synchronize data collection with scan sequences.

The pointing system operated continuously during the whole flight until well into the descent at around 2229:00 UTC,  $4.94 \times 10^4$  s after launch. It collected approximately 40 MB of downlinked data. An analysis of the data indicates that the system performed well, with all sensors operational throughout the flight. Instrument data were acquired during sunrise and for one complete limb scan before the command uplink capability was lost due to a receiver failure. Pointing performance in elevation met the required specifications during both limb and occultation modes. Pointing performance in azimuth did not meet specification goals but was adequate to obtain useful instrument datasets. A log of flight events is presented in Table 3.

### a. Gondola attitude data

The gondola was released with a  $12^\circ \text{ s}^{-1}$  azimuth rotation imparted by the launch truck and completed

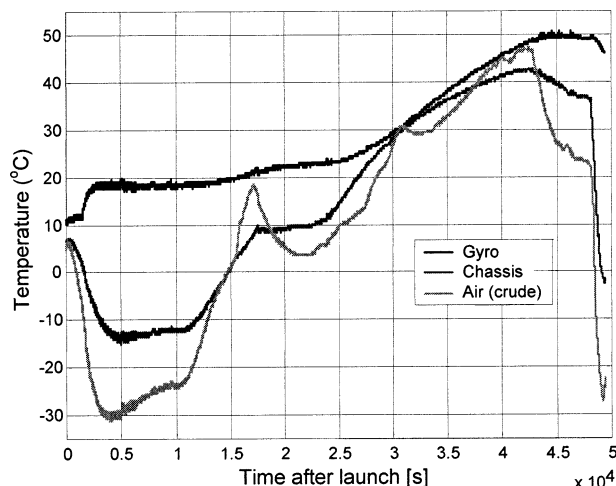


FIG. 7. Pointing system temperature variations during the flight.

several full rotations before settling down to a periodic yaw. The pointing system gained azimuth control over the payload 4000 s into the flight, losing control again briefly at 7920 s when the gondola reached float altitude. At launch a rapid  $5^\circ$  elevation pendulation at approximately 0.5 Hz developed. This quickly dissipated to a motion of only a few tenths of a degree within a few cycles. Elevation gyro measurements indicated that this low-level pendulation persisted until about 4800 s into the flight. This is likely attributable to motion at the azimuth pivot, driven by wind shear. During the rest of the flight, the elevation remained extremely stable, deviating less than  $0.05^\circ$  until descent.

The loss of telecommand prevented the shutdown of the pointing system prior to descent, and attitude data was recorded after termination and until the parachute deployed. This data indicated that the gondola yawed as it fell, reaching rates exceeding  $\pm 25^\circ \text{ s}^{-1}$ , and pendulated rapidly in elevation within approximately  $10^\circ$  of level pointing.

#### b. Environmental data

Figure 7 shows the pointing system temperature variations during the flight. At launch, the pointing system was at  $+7^\circ\text{C}$ , very close to the ambient air temperature. During the flight, the pointing system chassis (as measured near the gyro mount) ranged between  $-15^\circ\text{C}$  (occurring during ascent, 83 min after launch) and  $+43^\circ\text{C}$  (11.7 h after launch). The insulated gyro mount proved effective, substantially limiting the rate of change of the gyro drift, though the mount did not reach the initial  $30^\circ\text{C}$  set-point temperature for nighttime operation, suggesting that some of the controller values may need adjustment. Loss of command capability prevented the set-point value from being increased for daytime operation. An analysis of occultation pointing data and filter residuals, acquired when the gyro was not used

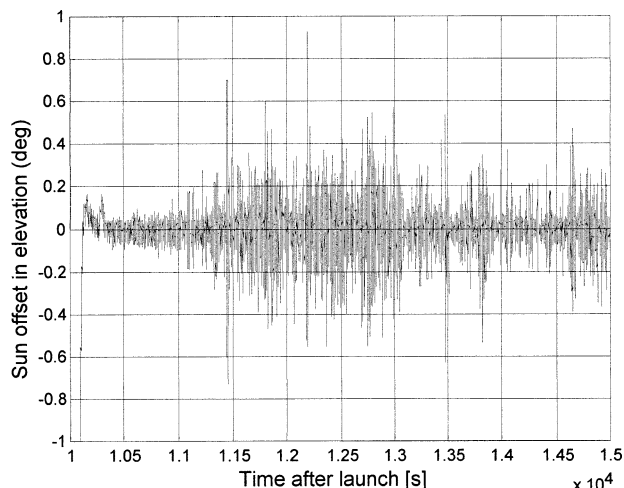


FIG. 8. Sun-sensor elevation offset during sunrise.

for elevation control, indicated that the estimator was able to track the change in gyro drift during the entire flight, despite a slow rise in gyro temperature throughout the mission.

#### c. Occultation data

The sunrise was acquired at 1134:00 UTC ( $1.01 \times 10^4$  s after launch), and the pointing system was left in Sun-pointing mode until 1255:20 (4880 s in total). Pointing performance is estimated to be  $\pm 0.086^\circ$  ( $1\sigma$ ) in elevation and  $\pm 3.1^\circ$  ( $1\sigma$ ) in azimuth. Figures 8 and 9 show the Sun offset from the pointing system's line of sight as measured by the Sun sensors (note that the Sun sensors have nonlinear gains, and computed angles will only be accurate within a few degrees of zero). Initial SPS instrument-data analysis indicates that a set of high quality solar-absorption spectra was collected, which is presented in Fig. 10.

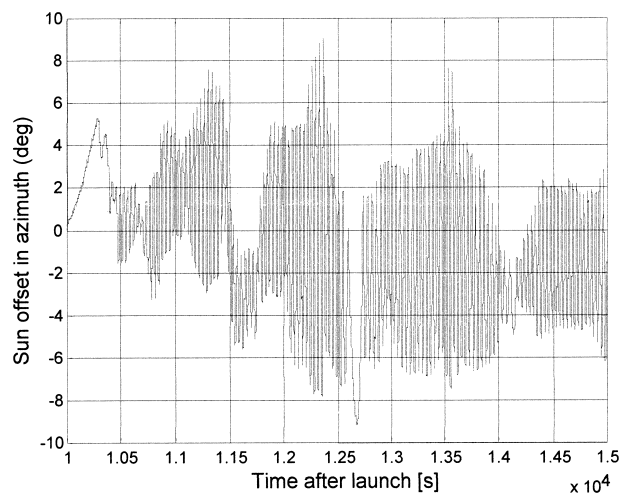


FIG. 9. Azimuth-pointing performance during sunrise.

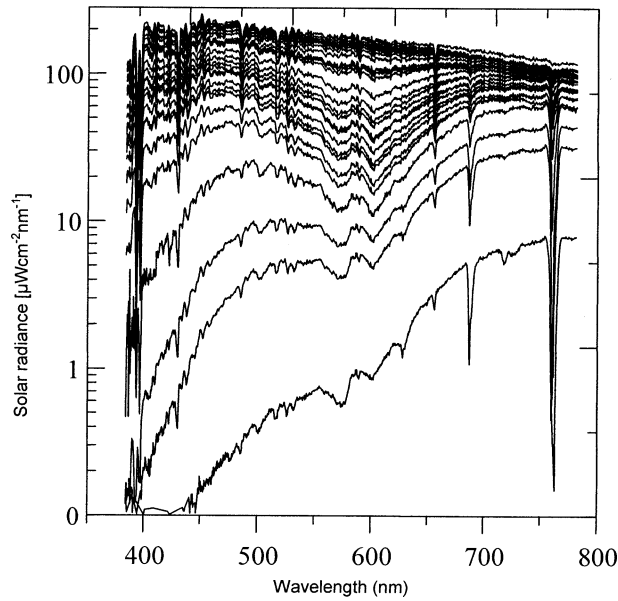


FIG. 10. Occultation data collected by the SPS instrument mounted on the pointing platform during sunrise (C. Nowlan 2001, personal communication).

*d. Limb-scanning data*

Two attempts to engage a limb-scanning mode were made prior to the complete loss of the gondola command uplink. The first was engaged at 1353:40 UTC ( $1.85 \times 10^4$  s after launch) but was terminated when control of the SPS instrument was inadvertently switched from the pointing system back to ground control by the launch contractor. The second attempt was initiated at 1422:00 UTC ( $2.02 \times 10^4$  s after launch), and a complete down/up scan sequence was performed until 1522:00 UTC ( $2.38 \times 10^4$  s after launch) according to a hard-coded limb table (calculated for 35 km). Pointing performance during the limb scan was  $\pm 0.072^\circ$  ( $1\sigma$ ) in elevation and

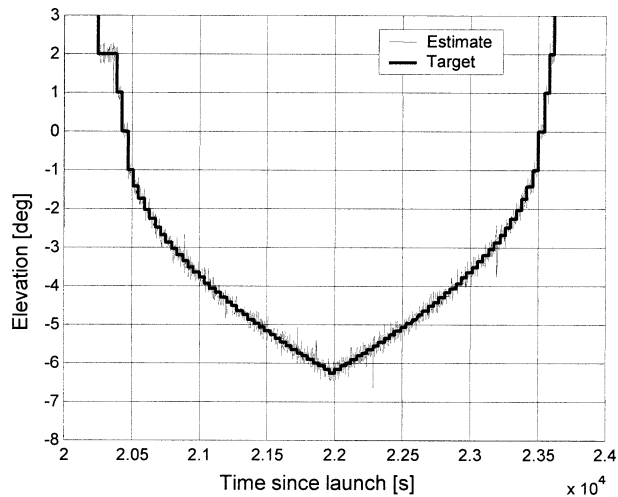


FIG. 11. Pointing-table elevation during complete limb scan.

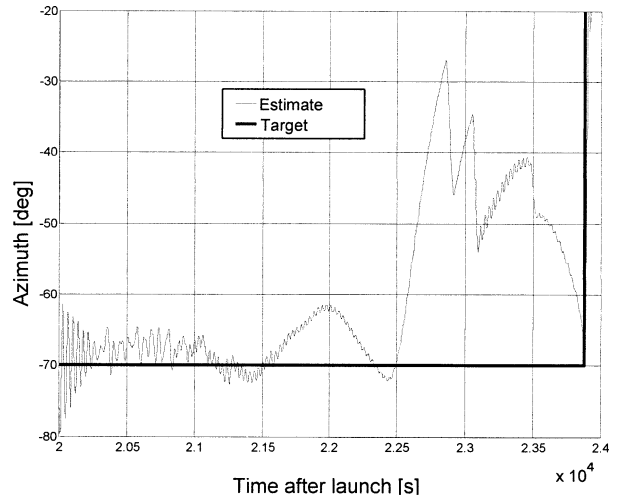


FIG. 12. Azimuth variation during complete limb scan.

$\pm 2.8^\circ$  ( $1\sigma$ ) in azimuth (during most of the scan and until a ground commanded change in the azimuth PID parameters caused the pointing system to lose track). Figures 11 and 12 show the estimated attitude of the pointing table and the required or target attitude.

Figure 13 shows an enlargement of a section of the limb scan, depicting periodic bursts of high-frequency error in the elevation estimate, occurring too rapidly to be real. This artifact is attributable to interference affecting the tilt sensor and gyro (discussed later). Despite this artifact, elevation pointing meets the  $\pm 0.1^\circ$  ( $1\sigma$ ) requirement. Further, the raw encoder data indicates that the actual pointing performance exceeds the estimate, as the system does not respond immediately to the rapid fluctuations during noise events.

*e. Pointing performance*

Elevation pointing met the required performance target of  $\pm 0.1^\circ$  ( $1\sigma$ ) in both pointing modes. Video footage

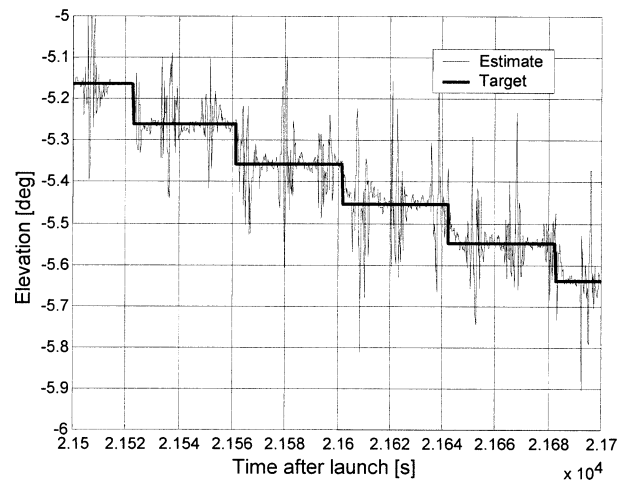


FIG. 13. Enlarged section of limb-scan elevation performance.

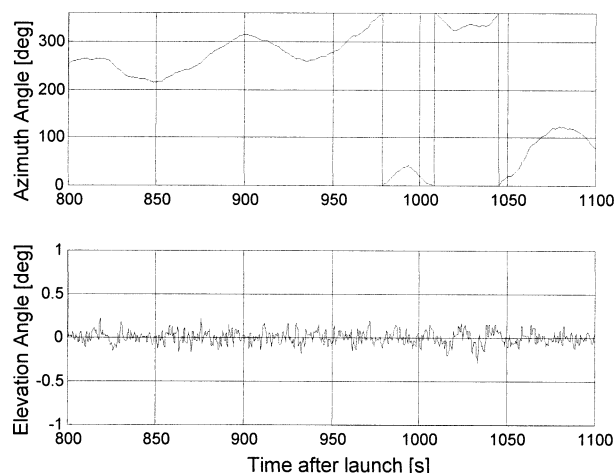


FIG. 14. Reprocessed azimuth and elevation angles 800–1100 s after launch.

from a camera mounted on the pointing system elevation stage and taken during both pointing modes provided an independent corroboration of relative elevation performance. Azimuth-pointing performance was less accurate: the system was able to hold azimuth to within a degree (peak to peak) during some mission phases but barely controlled azimuth after any significant maneuver. The poor performance is likely due to the inability of a simple PID control law to control azimuth pointing by applying torques to a flexible flight train.

During the balloon ascent, the tilt sensor and gyro both acquired a 12-s periodic corruption that was identified as being exactly synchronous with the UV-sonde transmissions. The corruption was most noticeable on the tilt sensor, causing a  $\pm 0.4^\circ$  periodic artifact in elevation data, and it occurred suddenly in the data from 1031:05 UTC (6405 s after launch). Arcing of a 600-V nonpressurized electrical circuit within the sonde may have caused this interference.

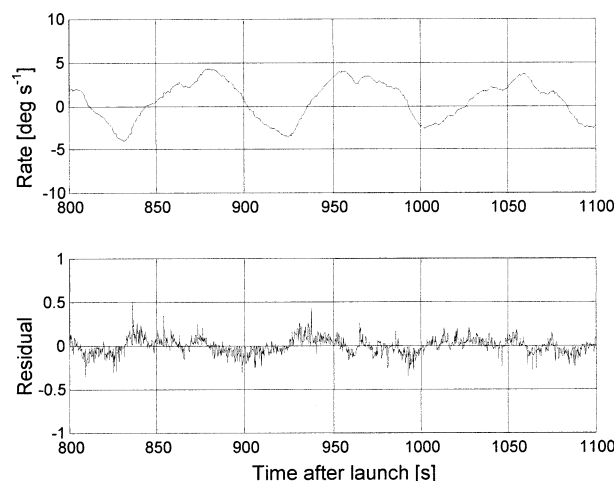


FIG. 15. Azimuth gyro measurement and reprocessed estimator residual, 800–1100 after launch.

#### f. Attitude estimation

The Kalman estimator employed to estimate payload attitude and gyro drift during limb scanning performed relatively well, producing good data at most attitudes. The elevation estimates suffered from periodic corruption caused by the interference described above, but the fusion of other sensor data reduced the amplitude of this corruption, and the estimator remained very stable in this axis. The estimator also appeared to track azimuth well at most attitudes, using the magnetometer to correct for gyro drift. There were, however, some particular azimuth angles where the azimuth estimates were unstable. This occurred because the fading-memory average observation was inadvertently applied only to the elevation axis rather than to both axes, making the attitude state vector unobservable at some azimuth orientations. This problem was rectified in postprocessing of the flight data. Figure 14 shows the motion 800 s after launch, during balloon ascent as postanalyzed by a Kalman filter. Figure 15 shows the corresponding azimuth gyro measurement and the estimator residual (the difference between the estimator prediction and the actual measurement). These figures indicate that the payload has a periodic 80-s yaw, most likely caused by a twisting of the flight train.

## 10. Conclusions

A conventional processing platform coupled with a standard operating system, high-level software, and off-the-shelf integrated sensor packages allowed the rapid development of a complex balloon-borne system. The use of a conventional computing platform eliminated the need for specialist digital electronic support and accelerated the development. The graphical interface language (Labview) proved exceptionally suited to this type of system development and had an extremely short learning curve, enabling nonspecialists to develop code modules with only a few days of training. The modularized sensor hardware allowed individual components to be tested early in the development and reduced programmatic development time and risk.

The pointing system performed well during its first flight, and both Sun-occultation and limb-scan instrument data were obtained before a failure of the balloon receiver severed the uplink command capability. With the exception of the azimuth-pointing requirement, the system met all of the design goals and performed nominally during the 14-h mission.

The azimuth performance was severely affected by the undamped torsional flexure mode of the flight train, which the PID controller failed to control adequately. This caused the azimuth angle to oscillate about the required pointing direction. This problem might be overcome using the existing suspension hardware, by implementing a more sophisticated digital controller tuned to avoid exciting the flexure mode, but the presence of

a low-frequency harmonic in the dynamics and stiction in the azimuth bearing will always complicate control. A more practical approach might be to include an additional azimuth pivot in the flight train, above the mass boom, to decouple the flight-train dynamics. The mass boom, top mount, and pivot would then behave like a crude momentum wheel, opposing torques applied to rotate the gondola by storing angular momentum. Bearing stiction can be avoided by operating the boom about nonzero angular speeds. The technique would be similar to that used by Kopp and Huguenin (1995) for the Geneva gondola. Further automation would also be desirable, to enable the pointing system to command instrument-data acquisition and to gather data during periods of complete communication blackout.

*Acknowledgments.* The research described here was jointly funded by the Canadian Space Agency and the Meteorological Service of Canada. SPS data was provided by Caroline Nowlan. We would like to thank the balloon-launch contractor Scientific Instrumentation Ltd. (SIL), of Saskatoon, Canada, for their support during the project. We are particularly grateful to Dr. C. Thomas McElroy (MSC), Prof. Barth Netterfield (University of Toronto), and the reviewers of this paper for their helpful advice and guidance.

## REFERENCES

- Abbas, M. M., M. J. Glenn, V. G. Kunde, J. Brasunas, B. J. Conrath, W. C. Maguire, and J. R. Herman, 1987: Simultaneous measurement of stratospheric O<sub>3</sub>, H<sub>2</sub>O, CH<sub>4</sub>, and N<sub>2</sub>O profiles from infrared limb thermal emissions. *J. Geophys. Res.*, **92** (D7), 8343–8353.
- Brasunas, J. C., V. G. Kunde, and L. W. Herath, 1988: Cryogenic Fourier spectrometer for measuring trace species in the lower atmosphere. *Appl. Opt.*, **27**, 4964–4974.
- Campbell, J. K., S. P. Synnott, and G. J. Bierman, 1983: Voyager orbit determination at Jupiter. *IEEE Trans. Autom. Control*, **AC-28**, 256–268.
- Carlotti, M., A. Barbis, and B. Carli, 1989: Stratospheric ozone vertical distribution from far-infrared balloon spectra and statistical analysis of errors. *J. Geophys. Res.*, **94** (D13), 16 365–16 372.
- Chance, K., W. A. Traub, D. G. Johnson, K. W. Jucks, P. Ciarpallini, R. A. Stachnik, R. J. Salawitch, and H. A. Michelsen, 1996: Simultaneous measurement of stratospheric HO<sub>x</sub>, NO<sub>x</sub>, and Cl<sub>x</sub>: Comparison with photochemical models. *J. Geophys. Res.*, **101** (D4), 9031–9043.
- Chui, C. K., and G. Chen, 1987: *Kalman Filtering with Real-Time Applications*. Springer Series in Information Sciences, Vol. 17, Springer-Verlag, 119 pp.
- Drummond, J. R., D. Turner, and A. Ashton, 1986: Attitude determination from a balloon-borne radiometer using two-sided limb scanning. *J. Atmos. Oceanic Technol.*, **3**, 59–66.
- Durrant-Whyte, H. F., 1998: *Integration, Coordination and Control of Multi-Sensor Robot Systems*. Kluwer Academic, 236 pp.
- Farmer, C. B., and O. F. Raper, 1977: The HF:HCl ratio in the 14–38 km region of the stratosphere. *Geophys. Res. Lett.*, **4**, 527–529.
- , —, B. D. Robbins, R. A. Toth, and C. Muller, 1980: Simultaneous spectroscopic measurements of stratospheric species: O<sub>3</sub>, CH<sub>4</sub>, CO, CO<sub>2</sub>, N<sub>2</sub>O, H<sub>2</sub>O, HCl and HF at northern and southern mid-latitudes. *J. Geophys. Res.*, **85** (C3), 1621–1632.
- , and Coauthors, 1990: Balloon intercomparison campaigns: Results of remote sensing measurements of HCl. *J. Atmos. Chem.*, **10**, 237–272.
- Hawat, T., and R. Torguet, 1996: The pointing and the sun-tracker system for the LPMA gondola. *Proc. SPIE*, **2739**, 112–119.
- , C. Camy-Peyret, and R. Torguet, 1998: Suntracker for atmospheric remote sensing. *Opt. Eng.*, **37**, 1633–1642.
- How, J., 1980: A small efficient sun pointing balloon gondola. *Proc. Fifth ESA-PAC Symp. on European Rocket and Balloon Programmes and Related Research*, Bournemouth, United Kingdom, ESA SP-152, 183–187.
- Jazwinski, A. H., 1970: *Stochastic Processes and Filtering Theory*. Mathematics in Science and Engineering, Vol. 64, Academic Press, 376 pp.
- Johnson, D. G., K. W. Jucks, A. Traub, and K. V. Chance, 1995: Smithsonian stratospheric far-infrared spectrometer and data reduction system. *J. Geophys. Res.*, **100** (D2), 3091–3106.
- Kalman, R. E., 1960: A new approach to linear filtering and prediction problems. *J. Basic Eng.*, 35–45.
- Kopp, E., and D. Huguenin, 1995: Swiss scientific balloon and sounding rocket experiments 1993–1995. *Proc. 12th ESA Symp. on Rocket and Balloon Programmes and Related Research*, Lillehammer, Norway, ESA SP-370, 17–21.
- Macher, G., 1995: The pointing and the star reference system of the MIPAS-B2 gondola Part 2: The star reference system. *Proc. 12th ESA Symp. on Rocket and Balloon Programmes and Related Research*, Lillehammer, Norway, ESA SP-370, 511–514.
- Maybeck, P. S., 1979: *Stochastic Models, Estimation and Control*. Mathematics in Engineering and Science, Vol. 141, Academic Press, 421 pp.
- McElroy, C. T., 1995: A spectroradiometer for the measurement of direct and scattered solar irradiance from on-board the NASA ER-2 high-altitude research aircraft. *Geophys. Res. Lett.*, **22**, 1361–1364.
- Michalsky, J. J., 1988: The astronomical almanacs algorithm for approximate solar position 1950–2050. *Sol. Energy*, **40** (3), 227–235.
- Murcray, D. G., 1984: Atmospheric transmission in the 750–2000 cm<sup>-1</sup> region. *J. Quant. Spectrosc. Radiat. Transfer*, **32** (5/6), 381–396.
- , F. J. Murcray, A. Goldman, F. H. Murcray, and J. J. Kusters, 1983: Balloon-borne remote sensing of stratospheric constituents. *Appl. Opt.*, **22**, 2629–2640.
- Oelhaf, H., and Coauthors, 1991: Remote sensing of trace gases with a balloon borne version of the Michelson interferometer for passive atmospheric sounding (MIPAS). *Proc. 10th ESA Symp. on Rocket and Balloon Programmes and Related Research*, Mandelieu-Cannes, France, ESA SP-317, 207–213.
- Payan, S., and Coauthors, 1999: Diurnal and nocturnal distribution of stratospheric NO<sub>2</sub> from solar and stellar occultation measurements in the arctic vortex: Comparison with models and ILAS satellite measurements. *J. Geophys. Res.*, **104** (D17), 21 585–21 593.
- Quine, B. M., 1997: *Spacecraft guidance systems: Attitude determination using star-camera data*. Ph.D. Thesis, University of Oxford, 186 pp.
- , J. Uhlmann, and H. F. Durrant-Whyte, 1995: Implicit Jacobians for linearised state estimation in nonlinear systems. *Proc. Amer. Control Conf.*, **3**, 1645–6.
- Robbins, D., and Coauthors, 1990: Ozone measurements from the balloon intercomparison campaign. *J. Atmos. Chem.*, **10**, 181–218.
- Roscoe, H. K., and Coauthors, 1990: Intercomparison of remote measurements of stratospheric NO and NO<sub>2</sub>. *J. Atmos. Chem.*, **10**, 111–144.
- Seefeldner, M., and C. Keim, 1995: The pointing and the star reference system of the MIPAS-B2 gondola. Part 1: The pointing system. *Proc. 12th ESA Symp. on Rocket and Balloon Programmes and Related Research*, Lillehammer, Norway, ESA SP-370, 505–510.

- Walraven, R., 1978: Calculating the position of the sun. *Sol. Energy*, **20**, 393–397.
- Waters, J. W., J. C. Hardy, R. F. Jarnot, and H. M. Pickett, 1981: Chlorine monoxide radical, ozone and hydrogen peroxide: Stratospheric measurements by microwave limb sounding. *Science*, **214**, 61–64.
- , ———, ———, and P. Zimmerman, 1984: A balloon-borne microwave limb sounder for stratospheric measurements. *J. Quant. Spectrosc. Radiat. Transfer*, **32** (5/6), 407–433.
- Watson, R. T., H. K. Roscoe, and P. T. Woods, 1990: The balloon intercomparison campaign: An introduction and overview. *J. Atmos. Chem.*, **10**, 99–110.
- Wertz, J. R., 1978: *Spacecraft Attitude Determination and Control*. Kluwer Academic, 858 pp.
- Zander, R., G. Roland, and L. Delbouille, 1977: Confirming the presence of hydrofluoric acid in the upper stratosphere. *Geophys. Res. Lett.*, **4**, 117–120.
- , N. Louisnard, and M. Bangham, 1990: Stratospheric methane concentration profiles measured during the balloon intercomparison campaigns. *J. Atmos. Chem.*, **10**, 145–158.